Systematic study on He isotopes with the antisymmetrized molecular dynamics plus generator coordinate method

N. Itagaki[1] and S. Aoyama[2]
[1]*RI Beam Science Laboratory, RIKEN (The Institute of Physical and Chemical Research), Wako, Saitama, 351-0198, Japan*
[2]*Information Processing Center, Kitami Institute of Technology, Kitami 090-8507, Japan*
(Received 20 July 1999; published 29 December 1999)

We study the structure of He isotopes systematically using a model in which the frameworks of the antisymmetrized molecular dynamics (AMD) and the generator coordinate method (GCM) are combined. The present AMD+GCM can reproduce basic features of the isotopes, for example halo structures in ^{6}He and tendency of the binding energies of the isotopes within relatively small number of basis functions. In ^{7}He, the importance of two configurations, ^{6}He-n and (^{4}He-n)$-2n$, is shown for the ground state. In ^{8}He, the calculated rms radius is smaller than the experimental one.

PACS number(s): 21.10.Dr, 21.60.Gx

I. INTRODUCTION

Recently, the development of experiments using unstable nuclear beams have enabled us to reveal a lot of exotic properties of neutron-rich nuclei close to the neutron dripline [1]. One such property is a so-called neutron halo structure consisting of a cloud of weakly bound valence neutrons around a core nucleus [2]. The wave function of a valence neutron with an extremely small binding energy has large spatial distribution and a long tail. For He isotopes, ^{6}He with a large root mean square (rms) radius [2] has been studied as a typical example of halo nuclei [3]. Such anomalous behaviors of weakly interacting valence neutrons around a core is observed not only in ^{6}He but also in other He isotopes. Therefore, now it is significant to study systematically the behavior of valence neutrons around a ^{4}He core in the isotopes. For example, recently, the excited states of ^{7}He ($E_x=2.9\pm0.3$ MeV [4], $E_x=3.2\pm0.2$ MeV [5]) are observed at very low energy region. The observed excited state has been analyzed to have a complicated $^4\mathrm{He}+n+n+n$ four-body structure [4]. Furthermore, also in ^{8}He, a large rms radius is observed [2], and it is also considered to have a similar halo (skin) structure.

In order to study structures of light neutron-rich nuclei beyond the three-body, several valuable approaches have been proposed up to now [6–15]. For example, the stochastic variational method (SVM) developed by Varga *et al.* [15] is one of the excellent methods to solve accurately few-body systems beyond three-body. However, when we include core excitation or extend to heavier systems, these few-body approaches make the computing time increase drastically. This may restrict the systematic study of light neutron-rich nuclei. On the other hand, the structure version of the antisymmetrized molecular dynamics (AMD) has been powerfully applied for systematic studies of neutron-rich nuclei [16]. However, since the wave function is essentially described by a single Slater determinant, this restriction makes it difficult to describe a halo structure as discussed in Ref. [16]. The attempt to superpose the Slater determinants has been performed, however, this has not satisfactorily worked to explain a large rms radius of ^{11}Be which is also a candidate for the halo nucleus. To improve this, recently a new method to combine the frameworks of the AMD and the Hartree-Fock method has been proposed [17].

In this paper, we propose a method which can describe the characteristic structure of valence neutrons including the halo (skin) structure quantitatively, which will be used for a systematic analysis of light neutron-rich nuclei. As a first step, we study He isotopes. We superpose the AMD wave functions based on the generator coordinate method (GCM). Since each AMD wave function (GCM basis function) is obtained through a variational process, the calculated energy converges rapidly even within small number of basis functions. Here, we superpose the AMD wave functions with different values of the rms radius, and the halo structure in He isotopes is reproduced.

In Sec. II, we briefly explain our model (AMD+GCM) by which we can quantitatively and systematically study many-body cluster systems. In Sec. III, the binding mechanism of He isotopes is discussed by applying the present method. Summary and conclusions are given in Sec. IV.

II. ^{4}He+VALENCE-NEUTRONS MODEL

To describe the structures of He isotopes systematically, we introduce a ^{4}He+valence-neutrons model in which the frameworks of the antisymmetrized molecular dynamics and the generator coordinate method (GCM) are combined. Total wave function ($|\Psi^{J^\pm}_{MK}\rangle$) is described as superposition of J^π projected AMD wave functions ($|\Phi^{J^\pm}_{MK}(\boldsymbol{Z}^{n(\beta)};\beta)\rangle$) based on the GCM as follows:

$$|\Psi^{J^\pm}_{MK}(\boldsymbol{Z})\rangle=\sum_\beta c^\beta|\Phi^{J^\pm}_{MK}(\boldsymbol{Z}^\beta;\beta)\rangle. \tag{1}$$

Here β represents numbers of the AMD basis functions, and the coefficients c^β are determined by diagonalizing the Hamiltonian matrix. The parameter $(\boldsymbol{Z}=\boldsymbol{Z}_1,\ldots,\boldsymbol{Z}_A)$ for

nucleons represents the centers of the Gaussian wave packets. Here, the parity and the angular momentum are projected to good quantum numbers,

$$|\Phi^{\pm}(\boldsymbol{Z})\rangle = \hat{P}^{J}_{MK}\hat{P}^{\pm}|\Phi(\boldsymbol{Z})\rangle, \tag{2}$$

$$\hat{P}^{\pm} = \frac{1}{2}(1 \pm \hat{P}^{(r)}), \tag{3}$$

$$\hat{P}^{J}_{MK} = \int d\alpha d(\cos\beta) d\gamma D^{J*}_{MK}(\alpha\beta\gamma)\exp(-i\alpha\hat{J}_z) \times \exp(-i\beta\hat{J}_y)\exp(-i\gamma\hat{J}_z)R(\alpha\beta\gamma). \tag{4}$$

Each AMD wave function in Eq. (2) for the A-nucleon system has the following form:

$$|\Phi(\boldsymbol{Z}_1\boldsymbol{Z}_2, \ldots, \boldsymbol{Z}_A)\rangle = \mathcal{A}[\phi_1\phi_2\cdots\phi_A], \tag{5}$$

$$\phi_i = \psi_i\chi_i, \tag{6}$$

where ϕ_i is the ith single particle wave function constructed from the spatial part ψ_i and the spin-isospin part χ_i. The spatial part is expressed by a Gaussian wave packet in coordinate representation,

$$\psi_i(\boldsymbol{r}) = \left(\frac{2\nu}{\pi}\right)^{3/4}\exp\left[-\nu\left(\boldsymbol{r} - \frac{\boldsymbol{Z}_i}{\sqrt{\nu}}\right)^2 + \frac{1}{2}\boldsymbol{Z}_i^2\right], \tag{7}$$

$$\propto \exp\left[-\nu(\boldsymbol{r} - \boldsymbol{R}_i)^2 + \frac{i}{\hbar}\boldsymbol{K}_i\cdot\boldsymbol{r}\right], \tag{8}$$

where complex parameters $\boldsymbol{Z}_i = \sqrt{\nu}\boldsymbol{R}_i + (i/2\hbar\sqrt{\nu})\ \boldsymbol{K}_i$ represent centers of the Gaussian wave packets and ν is the width parameter. In the present analysis, we assume a presence of an α cluster ($\boldsymbol{Z}_1 = \boldsymbol{Z}_2 = \boldsymbol{Z}_3 = \boldsymbol{Z}_4 = \boldsymbol{Z}_\alpha$) [18], then the model space becomes ^{4}He+valence neutrons:

$$|\Phi(\boldsymbol{Z}_\alpha, \boldsymbol{Z}_5, \ldots, \boldsymbol{Z}_A)\rangle = \mathcal{A}[\phi_\alpha(1234)\phi_5\cdots\phi_A]. \tag{9}$$

In this framework, the AMD wave functions with different intrinsic configurations are superposed based on the GCM. This is performed by constraining the AMD wave functions to have a fixed expectation value of some physical quantity, and by changing this constrained value, a lot of the GCM basis functions are generated. We constrain the rms radius of the total system. The diagonal elements of the Hamiltonian matrix become a function of parameter $\boldsymbol{Z}$,

$$E(\boldsymbol{Z}, \boldsymbol{Z}^*) \equiv \frac{\langle\Phi^{\pm}(\boldsymbol{Z})|\hat{H}|\Phi^{\pm}(\boldsymbol{Z})\rangle}{\langle\Phi^{\pm}(\boldsymbol{Z})|\Phi^{\pm}(\boldsymbol{Z})\rangle}. \tag{10}$$

We optimize these parameters, $\boldsymbol{Z}$ before the angular momentum projection by using the frictional cooling method in the AMD,

$$\frac{d\boldsymbol{Z}_i}{d\tau} = -\frac{\partial E}{\partial \boldsymbol{Z}_i^*}, \quad \frac{d\boldsymbol{Z}_i^*}{d\tau} = -\frac{\partial E}{\partial \boldsymbol{Z}_i}. \tag{11}$$

As shown in Ref. [16], by solving this cooling equation, the expectation value of the Hamiltonian (E) decreases as development of imaginary time τ, since the τ derivative of E is always negative,

$$\frac{dE}{d\tau} = \sum_{i=5}^{A}\frac{\partial E}{\partial \boldsymbol{Z}_i}\frac{d\boldsymbol{Z}_i}{d\tau} + \sum_{i=5}^{A}\frac{\partial E}{\partial \boldsymbol{Z}_i^*}\frac{d\boldsymbol{Z}_i^*}{d\tau}, \tag{12}$$

$$= -2\sum_{i=5}^{A}\frac{d\boldsymbol{Z}_i}{d\tau}\frac{d\boldsymbol{Z}_i^*}{d\tau} < 0. \tag{13}$$

During this optimization of parameters, parity of the system is projected to a good quantum number. We can constrain the value of an rms radius during the cooling process by introducing a Lagrange multiplier in Eq. (12),

$$\frac{d\boldsymbol{Z}_i}{d\tau} = -\frac{\partial E}{\partial \boldsymbol{Z}_i^*} + \eta\frac{\partial O}{\partial \boldsymbol{Z}_i^*}, \quad \frac{d\boldsymbol{Z}_i^*}{d\tau} = -\frac{\partial E}{\partial \boldsymbol{Z}_i} + \eta\frac{\partial O}{\partial \boldsymbol{Z}_i}, \tag{14}$$

where O is the expectation value of an rms radius. Here, the multiplier η is determined by the condition that the τ derivative of O is zero,

$$\frac{\partial O}{\partial \boldsymbol{\tau}} = \sum_{i=5}^{A}\frac{\partial O}{\partial \boldsymbol{Z}_i}\frac{\partial \boldsymbol{Z}_i}{\partial \boldsymbol{\tau}} + \text{c.c.} = \sum_{i=5}^{A}\frac{\partial O}{\partial \boldsymbol{Z}_i}\left\{-\frac{\partial E}{\partial \boldsymbol{Z}_i^*} + \eta\frac{\partial O}{\partial \boldsymbol{Z}_i^*}\right\} + \text{c.c.} = 0. \tag{15}$$

Therefore, the η value is determined from this equation

$$\eta = \frac{\sum_{i=5}^{A}(\partial O/\partial \boldsymbol{Z}_i)(\partial E/\partial \boldsymbol{Z}_i^*) + \text{c.c.}}{\sum_{i=5}^{A}(\partial O/\partial \boldsymbol{Z}_i)(\partial O/\partial \boldsymbol{Z}_i^*) + \text{c.c.}}. \tag{16}$$

The Hamiltonian operator $\hat{H}$ has the following form:

$$\hat{H} = \sum_{i=1}^{A}\hat{t}_i - \hat{T}_{\text{c.m.}} + \sum_{i>j}^{A}\hat{v}_{ij}, \tag{17}$$

where a two-body interaction $\hat{v}_{ij}$ includes the central part, the spin-orbit part and the Coulomb part. For the central part, we use a Volkov-type effective $N-N$ potential [19] as

$$V(r) = (W - MP^{\sigma}P^{\tau})[V_1\exp(-r^2/c_1^2) + V_2\exp(-r^2/c_2^2)], \tag{18}$$

where, $W = 1 - M$. For the spin-orbit term, we introduce the G3RS potential [20] as

$$V_{ls} = V_0\{e^{-d_1 r^2} - e^{-d_2 r^2}\}P(^3O)\vec{L}\cdot\vec{S}, \tag{19}$$

where $d_1 = 5.0\ \text{fm}^{-2}$, $d_2 = 2.778\ \text{fm}^{-2}$, $P(^3O)$ is a projection operator onto a triplet odd state, $\vec{L}$ is a relative angular momentum, and $\vec{S}$ is a spin ($\vec{S}_1 + \vec{S}_2$). The potential strength V_0 will be given in Table I.

TABLE I. The parameters for effective nucleon-nucleon interactions.

	V_1 (MeV)	V_2 (MeV)	c_1 (fm)	c_2 (fm)	M	V_0 (MeV)
En'yo 1	−83.34	144.86	1.60	0.82	0.56	900
Okabe 1	−60.65	61.14	1.80	1.01	0.60	2000
En'yo 2	−83.34	144.86	1.60	0.82	0.55	900
Okabe 2	−60.65	61.14	1.80	1.01	0.56	2000

III. RESULTS AND DISCUSSION

First, we study structures of He isotopes within a model space of a single Slater determinant in order to see validity of applying the AMD wave functions. For Li and Be isotopes, the applicability of the AMD has been already shown by En'yo, Horiuchi, and Ono. Basic properties of nuclei have been reproduced except for anomalous behaviors of single particle orbits such as a halo structure for example in ^{11}Li and ^{11}Be [16]. We compare four sets of the parameters for the Volkov potential as listed in Table I: En'yo 1 used in the original AMD in Ref. [16], and Okabe 1 used for an analysis on ^{9}Be in Ref. [21]. We introduce new parameters En'yo 2 and Okabe 2 whose Majorana exchange parameters are determined to reproduce the four neutron binding energy of ^{8}He (B.E.=3.11 MeV [22]).

In Fig. 1(a), we show the binding energies of He isotopes calculated within the bound state approximation. Both results with parameters En'yo 1 and Okabe 1 have shortcomings in comparison with experimental binding energies, by several MeV. That means a single Slater determinant may not be enough to describe valence neutron's motion around the core. Furthermore, it is impossible to find parameters which reproduce the binding energies systematically within a single Slater determinant. For example, in Fig. 1(a), using parameters En'yo 2 and Okabe 2 whose Majorana exchange parameters are modified to reproduce the four-neutron binding energy of ^{8}He, we cannot reproduce the binding energies of ^{5}He, ^{6}He, and ^{7}He.

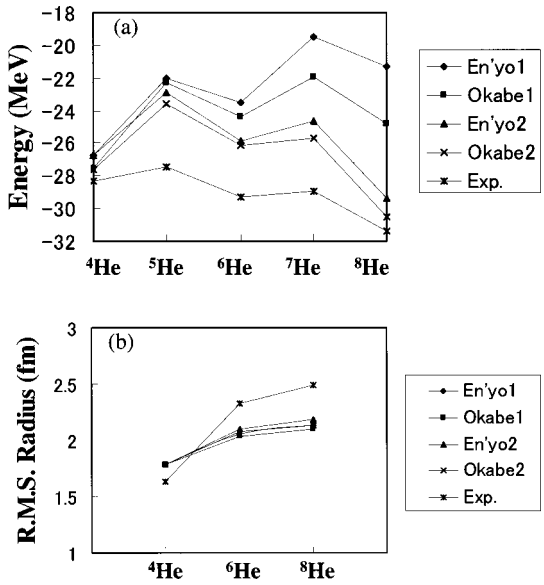

FIG. 1. (a) The binding energies of He isotopes with AMD and (b) the root mean square radii of He isotope with AMD.

In Fig. 1(b), we show rms radii of the He isotopes. All calculated radii are smaller than observed ones. To describe the loosely bound or unbound nature of valence neutrons around ^{4}He core, we should superpose Slater determinants. In Ref. [16], En'yo, Horiuchi, and Ono superposed a few Slater determinants for ^{11}Be, but that only has slightly increased the value of the rms radius. To reproduce the experimental large value of the rms radius, a much larger number of the basis functions is required, but that increases calculation time drastically. Therefore, the problem is how to choose effective basis functions. In this work, we superpose the AMD wave functions chosen through a simple variational procedure which will be explained below. We prepare the AMD wave functions corresponding to the energy minimal state under the constraint of the values of the rms radius. And we superpose all these functions generated by changing the constrained values of the rms radius (GCM). Here, the coefficients for the superposition are determined by diagonalizing the Hamiltonian matrix. This is an idea to describe the nuclear structure such as a halo within rather small number of basis functions.

Next, we investigate the validity of this procedure in ^{6}He. The AMD wave functions are used as basis functions of the GCM. The interaction used is Volkov No. 2 with a Majorana exchange parameter $M=0.58$. Figure 2(a) shows large energy gain of ^{6}He due to the superposition of the AMD wave functions as GCM basis functions, and the energy rapidly converges. The horizontal axis shows the number of basis functions which are superposed. Here, 1 on the horizontal axis corresponds to one basis function, which is calculated without the constraint of the value of an rms radius. And 2 on the horizontal axis shows the superposition of this basis function and one whose rms radius ($R_{\rm rms}$) is constrained to 2.15 fm. In the same way, 3 corresponds to the superposition of these basis functions and a new one with $R_{\rm rms}=2.20$ fm, and so on up to $R_{\rm rms}=2.60$ fm with step by 0.05 fm. Since the calculated energy shows rapid convergence, the framework we have introduced works well.

In Fig. 2(b), the energy of each basis function is shown. The horizontal axis represents the constrained value of the rms radius. The AMD wave function whose rms radius is constrained to 2.30 fm (this is close to the experimental value) gives the lowest energy after the angular momentum projection to 0^+. This 0^+ energy (−25.7 MeV) is lower than one obtained without the constraint (−24.7 MeV) by about 1 MeV. This shows that the approximation of the projection after variation in the simple AMD is much overcome by applying the constraint to the rms radius. When we perform the GCM calculation, the energy of the ground state becomes lower by 3 MeV. This is due to the reduction of the kinetic energy, and the valence neutrons have very spread spatial distribution.

Furthermore, in Fig. 2(c), we show the convergence of an rms radius to a large value when AMD wave functions are superposed as GCM basis functions. The value of the horizontal axis is the same as in Fig. 2(a). As seen in Fig. 2(c), the rms radius also converges near the experimental value

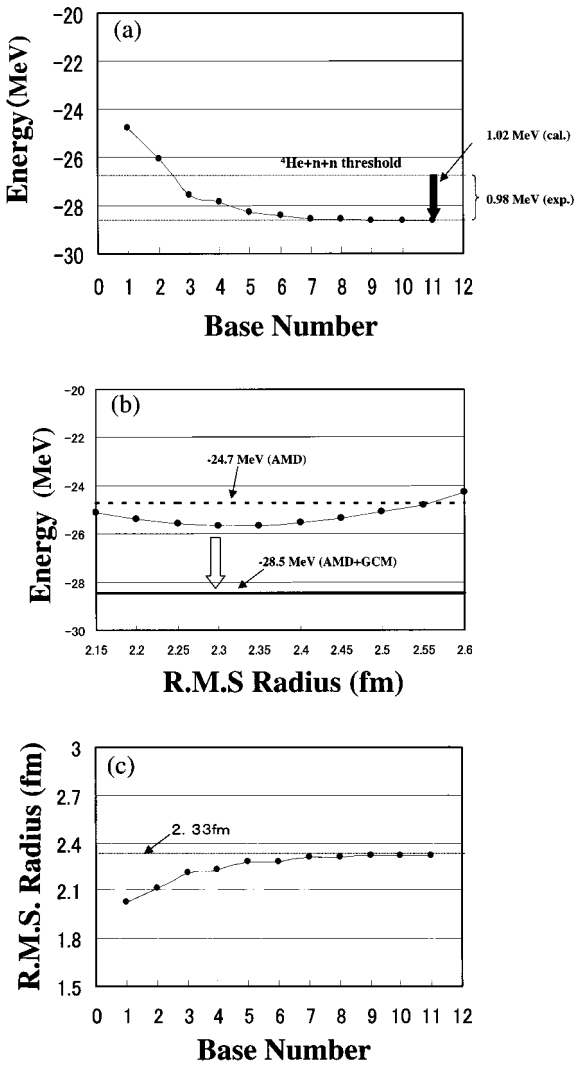

FIG. 2. (a) The convergence of energy for ^{6}He. The horizontal axis shows the number of basis functions superposed. (b) The 0^+ energy of each basis function. The horizontal axis is rms radius of each basis function. (c) The convergence of root mean square radius for ^{6}He. The horizontal axis is the same as (a).

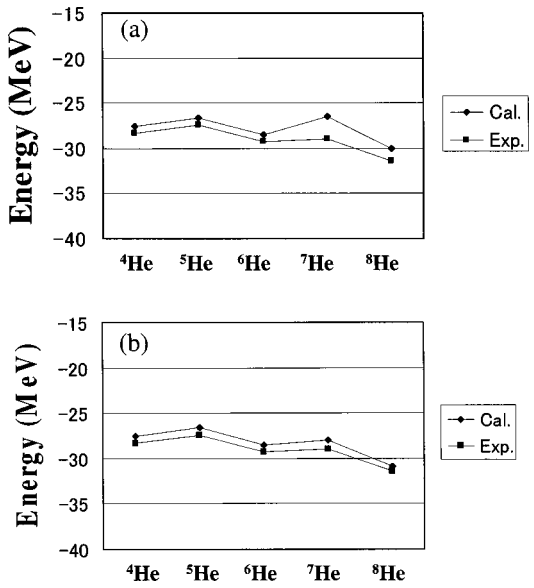

FIG. 3. (a) Binding energies of He isotopes with AMD+GCM (not including local energy minimum). (b) Binding energies of He isotopes with AMD+GCM (including local energy minimum).

when the binding energy reproduces the experimental value. Therefore, now we get the wave function which reproduces the binding energy and the rms radius simultaneously within rather small number of the basis functions. Here, it should be mentioned that the properties of spatially extended valence neutrons around ^{4}He core is essentially described, even if the present wave function is not an exact one because of the limited model space. However, it is difficult to compare the present result with the full space calculations, since the model space is truncated to only the set of optimal basis functions under the constraint of the rms radius. In fact, when we use the same Minnesota potential employed in the calculation by Csótó [8], we need the exchange parameter $u=1.1$ to have the observed binding energy of ^{6}He (u parameter in Ref. [8] is $u=0.98$), then more attractive central potential is required to have the same binding energy.

As far as the so-called underbinding problem in ^{6}He is concerned, in Ref. [8], the breaking of the α cluster has been shown to be significant in the case of ^{6}He ($t+t$ clusterization). Using the present framework, such effects of core-cluster breaking can easily be taken into account without any mathematical and computational difficulties. We have checked for ^{6}He that the α cluster breaking contributes to the increase of the binding energy by a few hundred keV. This energy gain is almost the same as the more accurate value obtained in Ref. [8]. Although this energy gain from the core-cluster-breaking effect in ^{6}He is $\sim$300 keV, it might be more critical for Li isotopes (e.g., α-t clustering effect), and this is our future problem.

Finally, we apply the present approach for He isotopes and discuss the binding mechanism. In Fig. 3(a), we show the binding energies of He isotopes. The interaction used is the same as that in Fig. 2. The systematic of the calculated binding energies shows good agreement with the experimental data except for ^{7}He. This insufficiency of ^{7}He is easily understood as follows. Since the ground state of ^{7}He is a resonance state above the ^{6}He-n threshold, the relative motion between ^{6}He and a valence neutron is mainly described by the present model. Then, the tail of one valence neutron is solved within a bound state approximation (the maximum constrained value of $R_{\rm rms}=2.6$ fm). On the other hand, the binding energy of ^{7}He from the ^{4}He$+n+n+n$ threshold is very small (B.E.$=0.54$ MeV [22]), and the ^{4}He-$2n$ motion in ^{6}He core is also important. This (^{4}He-n)$-2n$ configuration corresponds to a local energy minimum in the energy surface of ^{7}He, which is very near to the ground energy minimum ($\delta E=\sim 0.05$ MeV). Therefore, in Fig. 3(b), for ^{7}He, we calculate the binding energy including both configurations (the maximum value of $R_{\rm rms}=2.6$ fm.). Now the calculated binding energy of He isotopes reproduce the tendency of the experimental values. Here, similar modification of wave functions to include a local minimal configuration is done also for ^{8}He, though it does not make a drastic change

different from the case of ^{7}He. For ^{5}He and ^{6}He, we cannot find any local energy minimum. Although the calculated rms radius of ^{6}He ($E=-1.02$ MeV and $R_{\rm rms}=2.32$ fm) is close to the experimental values ($E=-0.98$ MeV [22] and $R_{\rm rms}=2.33$ fm [23], 2.48 fm [2]), that of ^{8}He ($E=-3.31$ MeV and $R_{\rm rms}=2.31$ fm) is smaller than the experimental value by ~ 0.2 fm ($E=-3.11$ MeV [22] and $R_{\rm rms}=2.49$ fm [23]). That is consistent with the accurate calculation by Varga *et al.* [15] ($E=-3.32$ MeV and $R_{\rm rms}=2.32$ fm), where interaction used is also modified from the original Minnesota potential to reproduce the experimental binding energy of ^{6}He.

For ^{5}He and ^{7}He, there exist problems to treat the unbound states. However, we checked the stability of the energy and the rms radius within the bound state approximation. Furthermore, since the ground state of ^{7}He is bound from the $^4\mathrm{He}+n+n+n$ threshold although it is unbound from the $^6\mathrm{He}+n$ threshold, the bound state approximation is expected to work for the two neutron decay mode and the three neutron decay modes. As far as the $^6\mathrm{He}+n$ decay mode is concerned, since the ground state energy of ^{7}He is below the centrifugal barrier of the p wave by about 1 MeV, the bound state approximation is expected to be valid.

IV. SUMMARY AND CONCLUSIONS

In summary, we have introduced a model for systematic analyses on light neutron-rich nuclei. As a first step, structures of He isotopes have been analyzed. In this model, the framework of the AMD is extended to describe the properties of weakly bound valence neutrons such as a halo structure. The AMD wave functions whose expectation values of the rms radius are constrained during the cooling process are prepared, and these energy minimal states with different constraint values are superposed based on the GCM. Because of this superposition, the large rms radius of ^{6}He is reproduced. Although the present model is rather simple, in which ~ 10 Slater determinants are superposed, the experimental tendency of the binding energies of He isotopes is reproduced except for ^{7}He. This insufficency of ^{7}He comes from the rack of basis functions which is intuitively understood as follows. According to the present procedure, ^{6}He-n relative motion is mainly solved. However, since the binding of ^{7}He is very weak from the $^4\mathrm{He}+n+n+n$ threshold (0.54 MeV [22]), it is also important to describe two valence neutrons' (di-neutron) motion against the core, which corresponds to a local minimum in the energy surface. Therefore, when we combine basis functions for both configurations (one neutron tail and two neutron tail), this underbinding problem is overcome. For ^{8}He, we obtain a smaller rms radius than the experimental ones. Since the present model can describe basic features of He isotopes systematically, as a future problem, we will apply the method for systematic analyses on Li and Be isotopes. The extension of the framework might be necessary to describe two center systems, for example $^7\mathrm{Li}(\alpha+t)$ and $^8\mathrm{Be}(\alpha+\alpha)$ because one center core picture is not valid so much as the case of He-isotopes.

ACKNOWLEDGMENTS

The authors would like to thank Professor K. Ikeda, Professor H. Horiuchi, and Professor K. Katō for helpful discussions, and Dr. A. Ohnishi and members of the nuclear theory group in Hokkaido University for various encouragements.

[1] *Proceedings of International Symposium on Physics of Unstable Nuclei*, Niigata [Nucl. Phys. **A588** (1995)]. *Proceedings of the Fourth International Conference on Radioactive Nuclear Beam*, Omiya [Nucl. Phys. **A616** (1997)].
[2] I. Tanihata, T. Kobayashi, O. Yamakawa, S. Shimoura, K. Ekuni, K. Sugimoto, N. Takahashi, T. Shimoda, and H. Sato, Phys. Lett. B **206**, 592 (1988).
[3] I. Tanihata, J. Phys. G **22**, 157 (1996).
[4] A.A. Korsheninnikov, M.S. Golovkov, A. Ozawa, E.A. Kuzmin, E.Yu. Nikolskii, K. Yoshida, B.G. Novatskii, A.A. Ogloblin, I. Tanihata, Z. Fulop, K. Kusaka, K. Morimoto, H. Otsu, H. Petrascu, and H. Tokanai, Phys. Rev. Lett. **82**, 3581 (1999).
[5] H.G. Bohlen *et al., VI International School-Seminar on Heavy Ion Physics, Dubna*, Russia, 1997, edited by Yu.Ts. (World Scientific, New York, 1997), p. 134.
[6] M.V. Zhukov, B.V. Danilin, D.V. Fedrov, J.M. Bang, I.J. Thompson, and J.S. Vaggen, Phys. Rep. **231**, 151 (1993).
[7] S. Aoyama, S. Mukai, K. Katō, and K. Ikeda, Prog. Theor. Phys. **93**, 99 (1995).
[8] A. Csótó, Phys. Rev. C **48**, 165 (1993).
[9] A. Csótó, Phys. Rev. C **49**, 3035 (1994).
[10] K. Arai, Y. Suzuki, and K. Varga, Phys. Rev. C **51**, 2488 (1995); K. Arai, Y. Suzuki, and R.G. Lovas, *ibid.* **59**, 1432 (1999).
[11] D. Baye, M. Kruglansky, and M. Vincke, Nucl. Phys. **A573**, 431 (1994).
[12] E. Hiyama and M. Kamimura, Nucl. Phys. **A588**, 35c (1995).
[13] P. Descouvemont, Phys. Rev. C **52**, 704 (1995).
[14] G.F. Filippov, K. Katō, and S.V. Korennov, Prog. Theor. Phys. **96**, 575 (1996).
[15] K. Varga, Y. Suzuki, and Y. Ohbayashi, Phys. Rev. C **50**, 189 (1994).
[16] Y. Kanada-En'yo, H. Horiuchi, and A. Ono, Phys. Rev. C **52**, 628 (1995).
[17] A. Doté, H. Horiuchi, and Y. Kanada-En'yo, Phys. Rev. C **56**, 1844 (1997).
[18] D. Brink, *Proceedings of the International School of Physics*, ''ENRICO FERMI,'' Course No. 36, p. 247.
[19] A.B. Volkov, Nucl. Phys. **74**, 33 (1965).
[20] N. Yamaguchi, T. Kasahara, S. Nagata, and Y. Akaishi, Prog. Theor. Phys. **62**, 1018 (1979).
[21] S. Okabe and Y. Abe, Prog. Theor. Phys. **61**, 1049 (1979).
[22] F. Ajzenberg-Selove, Nucl. Phys. **A490**, 1 (1988).
[23] I. Tanihata, D. Hirata, T. Kobayashi, S. Shimoura, K. Sugimoto, and H. Toki, Phys. Lett. B **289**, 261 (1992).